# Shift of Brewster's angle with two-dimensional materials and structures

Oleh Yermakov ®*

*V. N. Karazin Kharkiv National University, Kharkiv 61022, Ukraine
and Leibniz Institute of Photonic Technology, Jena 07745, Germany*

The Brewster effect has a number of applications in antireflection coatings, spectroscopy, and polarization optics, but its tunability is still of high demand. In this Letter, we discover a method of Brewster angle control with two-dimensional conducting layers. Namely, we analyze the angular shift of Brewster's angle depending on the surface conductivity of a two-dimensional layer. First, we derive the analytical model with exact conductivity-dependent solution. Then, we investigate the Brewster angle shift in the cases of monolayer graphene and plasmonic metasurface. Finally, we support our analytical results by the full-wave numerical simulations. The results obtained may find a plethora of applications in flat optical and planar photonic devices.

*Introduction.* Polarization is an inherent vectorial property of electromagnetic waves which defines the orientation of the electric and magnetic fields vectors in time. Two fundamental polarization states following directly from Maxwell's equations in homogeneous isotropic medium are transverse electric (TE) and magnetic (TM) linear polarizations [1]. The study of light polarization has a rich history that spans several centuries. An important milestone was achieved more than two centuries ago by David Brewster [2]. He has shown that TM-polarized light does not reflect from the interface between two media under certain incident angle. Several years later, this fact was supported by the analytical formulas, derived by A.-J. Fresnel, describing the incidence of light at optical interface [3]. In particular, Fresnel has derived and theoretically confirmed the peculiar observation of Brewster [4]. In this aspect, two identical definitions of Brewster's angle (BA) emerge defining it as (1) the zero-reflection angle in TM polarization and (2) the angle at which unpolarized light becomes linearly polarized (namely, TE polarized) in reflection [5]. Naturally, the applications of BA include polarization filters [6], antireflective coatings [7,8], spin-orbit photonics [9,10], sensing [11,12], microscopy of monolayers [13–15], and biological systems [16].

The control of BA with nanostructures has been intensively studied in recent years, in particular using surface roughness [17], randomly stratified dielectric media [18], or additional dielectric layer [19]. The manipulation via Mie-like electric and magnetic resonances in high-index all-dielectric nanostructures leads to the generalized Brewster's law [20,21]. Another way to manipulate the BA is to use the ultrathin two-dimensional (2D) materials. It has been theoretically pre-

dicted that using the 2D nonmagnetic conductive layer under the specific conditions, it is possible to achieve the Brewster effect for TE polarization even under normal incidence [22]. It has been shown that by varying the surface conductivity of graphene via the applied voltage the BA can be shifted by a few degrees [23,24]. The angular shift of the BA has also been analyzed for the multilayered graphene and other 2D materials, including stanene and silicene [25]. The phase-change materials demonstrate the promising platform for the tunable Brewster effect [26]. For most cases, the typical theoretically expected and experimentally measured shifts of BA do not exceed $10°$ (usually less than $5°$).

In this Letter, we derive the Fresnel coefficients for the case of the 2D conducting sheet at the interface. The condition and the exact analytical equation of the Brewster angle shifted due to the 2D layer. Using the developed analytical model, we analyze the BA's shift for the case of the monolayer graphene and the plasmonic metasurface (MS) in the terahertz (THz) and visible ranges, respectively. Finally, we verify the analytical results by full-wave simulations and propose the real design of the plasmonic metasurface based on the gold nanodisks exhibiting a BA shift of $16.6°$. The results obtained discover a new page of interest in the Brewster phenomenon caused by the rapid development of 2D materials and planar nanotechnologies.

*Model.* We consider the oblique incidence in the $xz$ plane of the TM-polarized plane wave from media "1" to "2" via the 2D interface described by the surface conductivity $\sigma$ [Fig. 1(a)]. The incident, reflected, and transmitted waves are characterized by the indices $i$, $r$, and $t$, respectively. The wave vectors are defined as follows:

$$\mathbf{k}^{\{i,r,t\}} = \left(k_x, 0, \{+, -, +\}k_z^{\{i,r,t\}}\right), \qquad (1)$$

where $k_x = n_1 k_0 \sin\theta$, $k_z^i = -k_z^r = n_1 k_0 \cos\theta$, and $k_z^t = n_1 k_0 \sqrt{n^2 - \sin^2\theta}$. Here, $\theta$ is the angle of incidence, $k_0 = 2\pi/\lambda$ is the wave vector in vacuum at the wavelength $\lambda$, $n = n_2/n_1$, and $n_{1,2} = \sqrt{\varepsilon_{1,2}\,\mu_{1,2}}$ is the refractive index of bottom (1) and upper (2) media, respectively. The boundary
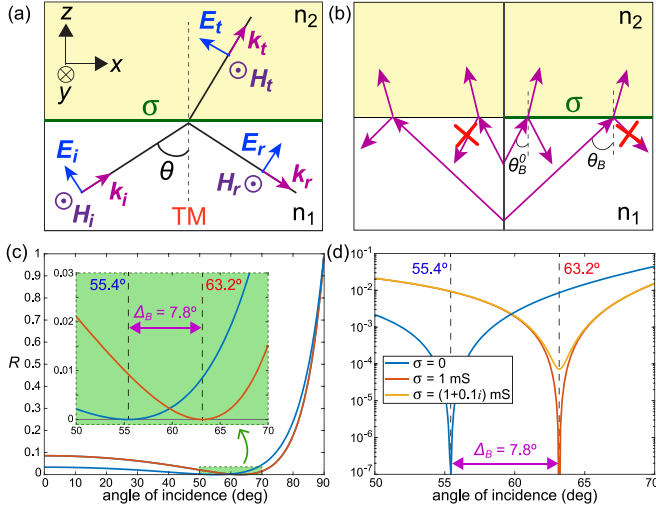
---

*oe.yermakov@gmail.com

FIG. 1. The concept of the angular shift of Brewster zero-reflection due to a 2D conducting interface. (a) The geometry of the problem shows the incidence of the TM-polarized wave under angle $\theta$ at a 2D layer described by the surface conductivity $\sigma$ and sandwiched between the media with refractive indices $n_1$ (bottom) and $n_2$ (top). (b) The schematic view of the angular shift of BA without (left) and with (right) the 2D conducting sheet. (c and d) The reflectance angular spectra of TM-polarized plane wave without [blue (left) line] and with [red (right) line] a 2D conducting sheet of $\sigma = 1$ mS in (c) linear and (d) logarithmic scale. The subfigure (d) shows the enlarged green area from (c). The yellow (light gray) line in (d) corresponds to a 2D conducting sheet with $\sigma = 1 + 0.1i$ mS.

conditions for the tangential components of electric and magnetic fields are

$$\mathbf{n}_{12} \times (\mathbf{E_2} - \mathbf{E_1}) = 0$$
$$\mathbf{n}_{12} \times (\mathbf{H_2} - \mathbf{H_1}) = \mathbf{J}, \quad (2)$$

where $\mathbf{n}_{12}$ is a normal vector from medium 1 to medium 2; $\mathbf{E}_1 = \mathbf{E}^i + \mathbf{E}^r$ is the full field in the bottom medium ($n_1$), which is the vectorial sum of the incident ($\mathbf{E}^i$) and reflected ($\mathbf{E}^r$) field, while the field in the upper medium $\mathbf{E}_2 = \mathbf{E}^t$ is just a transmitted field ($\mathbf{E}^t$); and $\mathbf{J}$ is the surface free current density, which is defined according to Ohm's law $\mathbf{J} = \sigma \mathbf{E}_{1,2}$, where $\sigma$ is normalized per $c/(4\pi)$. Applying Maxwell's equations and the boundary conditions (2), we derive the complex reflection and transmission coefficients defined as $r = \mathbf{H}^r/\mathbf{H}^i$ and $t = \mathbf{H}^t/\mathbf{H}^i$:

$$r = \frac{\dfrac{\varepsilon_2}{k_z^t} - \dfrac{\varepsilon_1}{k_z^i} + \dfrac{\sigma}{k_0}}{\dfrac{\varepsilon_2}{k_z^t} + \dfrac{\varepsilon_1}{k_z^i} + \dfrac{\sigma}{k_0}},$$

$$t = \frac{2\dfrac{\varepsilon_2}{k_z^t}}{\dfrac{\varepsilon_2}{k_z^t} + \dfrac{\varepsilon_1}{k_z^i} + \dfrac{\sigma}{k_0}}. \quad (3)$$

The total intensity-related reflectance and transmittance are defined as follows:

$$R = |r|^2, \quad T = \text{Re}\left(\frac{k_z^t/\varepsilon_2}{k_z^i/\varepsilon_1}\right)|t|^2. \quad (4)$$

Following the energy conservation law, the normal component of the Poynting vector should be conserved, so the additional factor for the transmittance emerges.

According to (3), we derive the Brewster angle condition for the case of 2D conducting sheet:

$$\frac{\varepsilon_2}{k_z^t} - \frac{\varepsilon_1}{k_z^i} + \frac{\sigma}{k_0} = 0. \quad (5)$$

It may be written in the following form:

$$\sigma = n_1\left(\frac{1}{\cos\theta_B} - \frac{n^2}{\sqrt{n^2 - \sin^2\theta_B}}\right), \quad (6)$$

where $\theta_B$ is the modified BA due to the presence of the 2D conducting layer. Equation (6) provides the value of $\sigma$ necessary to obtain the Brewster phenomenon at the angle $\theta = \theta_B$. One can notice that the shift of BA is possible due to the nonzero real part of the surface conductivity $\sigma$. Thus, the mechanism of BA shift is based on reflection compensation by absorption in the 2D layer.

Besides, Eq. (5) may also be exactly represented via the following quartic equation:

$$\frac{\tilde{\sigma}^2}{\eta}x^4 - \frac{2\tilde{\sigma}}{\eta}x^3 + [\tilde{\sigma}^2 - (1 + n^2)]x^2 - 2\tilde{\sigma}x + 1 = 0, \quad (7)$$

where $x = \cos\theta_B$, $\tilde{\sigma} = \sigma/n_1$, and $\eta = n^2 - 1$. One can notice that under $\sigma = 0$, we come to the standard formula $\theta_B = \theta_B^0 = \text{atan } n$. Note that the special case of $n_2 \gg n_1$ leads to the great simplification of the expression for $\theta_B$:

$$\cos\theta_B = \frac{\cos\theta_B^0}{1 + \tilde{\sigma}\cos\theta_B^0}. \quad (8)$$

Finally, we introduce and further study the angular shift of BA $\Delta_B$ defined as

$$\Delta_B(n_1; n_2; \sigma) = \theta_B(n_1; n_2; \sigma) - \theta_B^0(n_1; n_2). \quad (9)$$

*Results.* In the following, we consider the incidence from the air on the 2D layer on the quartz substrate ($n_1 = 1$, $n_2 = 1.45$). In this case, the standard BA is equal to $\theta_B^0 = 55.4°$. In order to demonstrate the concept of the angular BA, we consider the reflectances of plane wave with (1) zero (no 2D conducting layer), (2) real, and (3) complex surface conductivities [Figs. 1(c) and 1(d)]. Namely, we demonstrate the angular BA of 7.8° with $\sigma = 1$ mS. One can notice that the introduction of the imaginary part of surface conductivity does not change the value of the modified BA, but decreases the degree of the reflection suppression [Fig. 1(d)]. Then, we consider two cases of real 2D conducting sheets: graphene monolayer in the THz range and plasmonic MS in the visible spectrum.

In the terahertz spectral range at room temperature and under typical doping levels, the optical conductivity of the graphene monolayer is mostly dominated by a term related to the intraband electronic transitions [27,28]

$$\sigma_g = \frac{4i\sigma_g^0}{\pi}\frac{E_F}{\hbar(\omega + i\gamma_g)}, \quad (10)$$

where $\sigma_g^0$ mS is the universal optical conductivity of graphene, $E_F$ is the Fermi energy, $\gamma_g$ is the relaxation rate, $\omega$ is the operational angular frequency, and $\hbar$ is the reduced Planck constant.
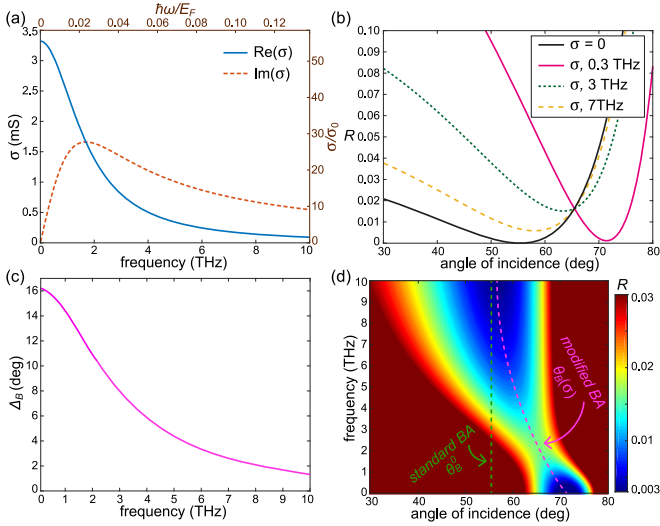
FIG. 2. The shift of Brewster's angle for a monolayer graphene layer. (a) The dispersion of real [blue (solid) line] and imaginary [red (dashed) line] parts of the surface conductivity according to (10). (b) The reflectance spectra for without (black line) and with a 2D conducting sheet for different frequencies [color (gray) lines]. (c) The dependence of the shift of BA on the frequency. (d) The dependence of the reflectance on the frequency and the angle of incidence. The green (vertical) and magenta (curve) dashed lines correspond to the standard and modified BA, respectively.
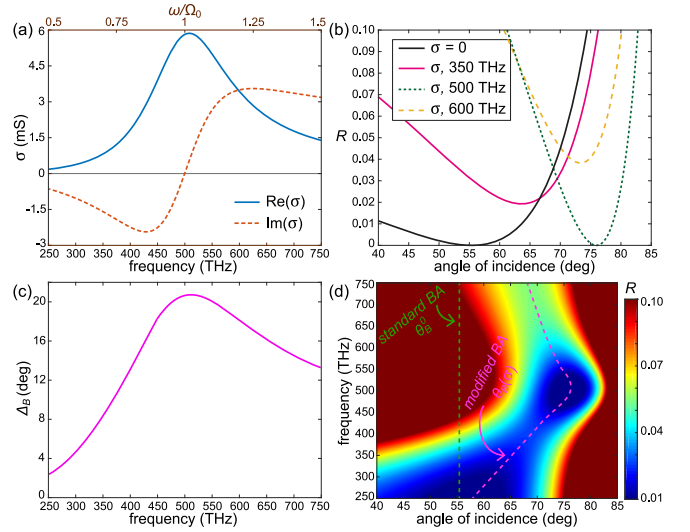


FIG. 3. The shift of Brewster's angle for a plasmonic metasurface. (a) The dispersion of real [blue (solid) line] and imaginary [red (dashed) line] parts of the surface conductivity according to (11). (b) The reflectance spectra for without (black line) and with 2D conducting sheet for different frequencies [color (gray) lines]. (c) The dependence of the shift of BA on the frequency. (d) The dependence of the reflectance on the frequency and the angle of incidence. The green (vertical) and magenta (curve) dashed lines correspond to the standard and modified BA, respectively.

The following parameters have been used [28]: $E_F = 0.3$ eV, $\gamma_g = 7$ meV, and $\sigma_g^0 = e^2/(4\hbar) = 608.5$ mS.

The dispersion of surface conductivity for the graphene monolayer in the THz range is shown in Fig. 2(a). One can notice that the real part of the surface conductivity decreases with the frequency, while the imaginary part is near zero at low frequencies and has the local maximum in the vicinity of 1.7 THz. Therefore, one can distinguish three regimes depending on the frequency: (1) the maximum shift is expected for the low frequencies (typically, less than 1 THz), while the real part is close to its maximum value and the imaginary part is close to zero; (2) the lowest level of reflection suppression is observed near the peak of the imaginary part of the conductivity (in the range from 1 to 3 THz); and (3) the shift is negligible as far as the surface conductivity tends to zero for large frequencies (namely, both the real and imaginary parts of the surface conductivity are less than 1 mS for frequencies greater than 5 THz). The corresponding reflectance spectra are shown in Fig. 2(b). As a consequence, the shift of BA decreases smoothly with the frequency, dropping by 10 times from the value of about $16°$ at 0.1 THz to $1.6°$ at 10 THz [Fig. 2(c)]. The dependence of the reflectance on the frequency and angle of incidence explicitly manifests the modified BA characterized by the reflectance dip [Fig. 2(d)]. It can be seen that in the case of the monolayer graphene, the modified BA is almost coincident with the standard BA at high frequencies and gradually shifts to the larger angles with decreasing frequency, reaching the maximum shift of BA of about $16°$ at low frequencies. The surface conductivity of the plasmonic metasurface may be well approximated with the

Drude-Lorentz formula [29,30]

$$\sigma_{\mathrm{ms}} = \frac{i\,\sigma_{\mathrm{ms}}^0\,\omega^2}{\omega^2 - \Omega_0^2 + i\gamma_{\mathrm{ms}}\,\omega}, \qquad (11)$$

where $\sigma_{\mathrm{ms}}^0$ is amplitude of surface conductivity, $\omega$ is the operational angular frequency, $\Omega_0$ is the resonant frequency, and $\gamma_{\mathrm{ms}}$ is the bandwidth of resonance. The following parameters, which correlate well with those of the Ref. [31], were used: $\Omega_0/(2\pi) = 500$ THz, $\gamma_{\mathrm{ms}}/(2\pi) = 175$ THz, and $\sigma_{\mathrm{ms}}^0/(2\pi) = 0.332$ mS.

The typical dispersion of the surface conductivity for the plasmonic MS in the visible frequency range is shown in Fig. 3(a). The resonance of the plasmonic MS at 500 THz is characterized by the peak and zero of the real and imaginary parts of the surface conductivity, respectively. Therefore, it is easy to predict the maximum shift of BA at the resonance of the plasmonic MS. At lower and higher frequencies, the shift of BA and the reflection suppression are less than at the resonance owing to the real and imaginary parts of the conductivity, respectively, as it can be seen at the reflectance spectra in Fig. 3(b). As a result, the shift of BA increases with the frequency up to the maximum value of about $21°$ corresponding to the resonance of plasmonic MS, and then it smoothly drops with further frequency increase after the resonance [Fig. 3(c)]. The nonmonotonic dependence of the modified BA of reflectance on frequency and angle of incidence, characterized by the dip in reflectance, is shown in Fig. 3(d). The modified BA always differs from the standard BA due to the high values of optical conductivity, reaching the maximum shift of BA at resonant frequency.
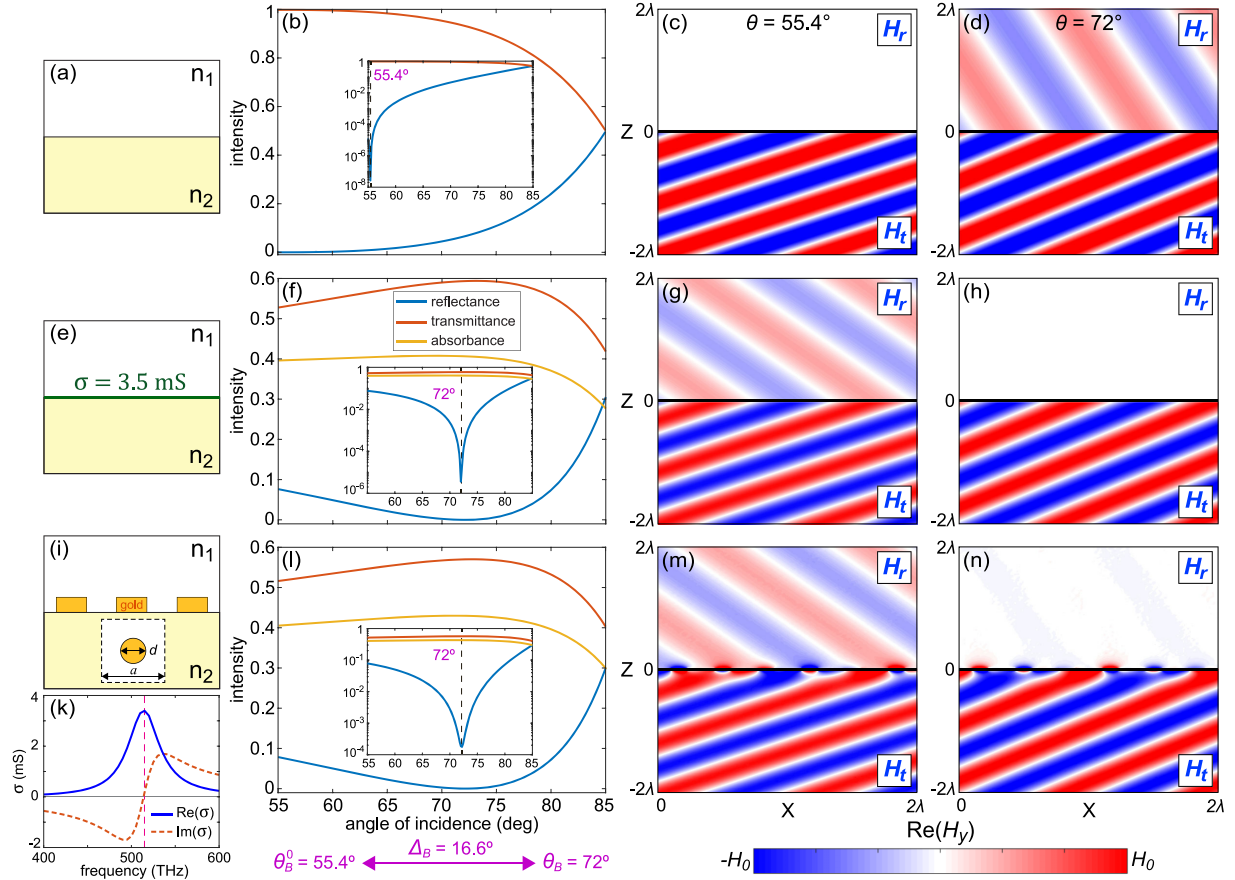
FIG. 4. The shift of Brewster's angle with a 2D conducting interface and a real design of plasmonic metasurface. The angular dependence of the reflectance (bottom line), transmittance (top line) and absorbance (middle line) (b), (f), and (l), and the spatial distributions of the reflected (top half-plane) and transmitted (bottom half-plane) magnetic fields (c), (d), (g), (h), (m), and (n) at the angles 55.4° (c), (g), and (m) and 72° (d), (h), and (n) corresponding to the BA for the cases of (a)–(d) nonconducting interface, (e)–(h) conducting interface, and (i)–(n) plasmonic MS based on gold nanodisks at the frequency of 515 THz schematically shown in (a), (d), and (i), respectively. The extracted surface conductivity and unit cell design of plasmonic metasurface are shown in (k) and as the insert in (i), respectively. The inserts in (b), (f), and (l) show the intensity-related parameters in the logarithmic scale. The BA shift caused by the 2D conducting layer (e)–(h) and plasmonic MS (i)–(n) is about 16.6°.

Figure 4 provides the verification of the analytical results via the full-wave numerical simulations based on the finite-element method in the frequency domain. First, we calculated the reflectance ($R$), transmittance ($T$), and absorbance ($A = 1 - R - T$) of the TM-polarized wave incident at the interface without 2D conducting layer [Figs. 4(a) and 4(b)] and with [Figs. 4(e) and 4(f)] a 2D conducting layer of $\sigma = 3.5$ mS and the plasmonic MS representing the square periodic array of gold nanodisks [Figs. 4(i) and 4(l)]. The dispersion of the thin gold films is taken from Ref. [32]. The period of plasmonic MS, the diameter, and the thickness of the nanodisks are 200, 80, and 25 nm, respectively [Fig. 4(i)]. Its surface conductivity extracted from the reflectance calculations [31] is shown in Fig. 4(k) and gives $\sigma = 3.4 + 0.17i$ (mS) at the frequency of 515 THz. The first case without a 2D conducting interface corresponds to Fresnel equations [1], while other two cases with a 2D conducting interface and plasmonic MS demonstrate the shift of BA from 55.4° to 72° [Figs. 4(f) and 4(l)]. The corresponding spatial distributions of the reflected and transmitted magnetic fields at these angles are shown in Figs. 4(c) and 4(d), 4(g) and 4(h), and 4(m) and 4(n).

We observe the suppression of the reflected magnetic field at $\theta = 72°$ for the cases of conducting structures at the interface. As it was previously discussed, this effect is supported by the absorbance compensation at the level of 40% of the initial intensity [Figs. 4(f) and 4(l)].

*Conclusion.* To conclude, we derived the analytical formulas of Brewster's angle for the case of a 2D conducting interface and analyzed the cases of a monolayer graphene layer and plasmonic metasurface. For the last case, we supported the analytical investigations by the numerically calculated magnetic fields. To the best of our knowledge, the predicted shift of BA of 16.6° for the real design of plasmonic nanostructure is the high-record value. Moreover, the recent approaches in the development of 2D materials [33,34] and the engineering of plasmonic anisotropic metasurfaces [31] including deep learning techniques [35,36] open new horizons for BA-related phenomena and applications.

[1] M. Born and E. Wolf, *Principles of Optics: Electromagnetic Theory of Propagation, Interference and Diffraction of Light* (Elsevier, New York, 2013).

[2] D. Brewster, On the laws which regulate the polarisation of light by reflexion from transparent bodies, Phil. Trans. R. Soc. Lond. **105**, 125 (1815).

[3] A. Fresnel, Note sur le calcul des teintes que la polarisation développe dans les lames cristallisées, Ann. Chim. Phys. **17**, 102 (1821).

[4] J. Z. Buchwald, *The Rise of the Wave Theory of Light: Optical Theory and Experiment in the Early Nineteenth Century* (University of Chicago, Chicago, 1989).

[5] A. Lakhtakia, Would Brewster recognize today's Brewster angle? Opt. News **15**, 14 (1989).

[6] R. Magnusson, D. Shin, and Z. Liu, Guided-mode resonance Brewster filter, Opt. Lett. **23**, 612 (1998).

[7] D. Shin, Z. Liu, and R. Magnusson, Resonant Brewster filters with absentee layers, Opt. Lett. **27**, 1288 (2002).

[8] H. Fan, J. Li, Y. Lai, and J. Luo, Optical Brewster metasurfaces exhibiting ultrabroadband reflectionless absorption and extreme angular asymmetry, Phys. Rev. Appl. **16**, 044064 (2021).

[9] H. Luo, X. Zhou, W. Shu, S. Wen, and D. Fan, Enhanced and switchable spin Hall effect of light near the Brewster angle on reflection, Phys. Rev. A **84**, 043806 (2011).

[10] J. B. Götte and M. R. Dennis, Limits to superweak amplification of beam shifts, Opt. Lett. **38**, 2295 (2013).

[11] K. V. Sreekanth, P. Mahalakshmi, S. Han, M. S. Mani Rajan, P. K. Choudhury, and R. Singh, Brewster mode-enhanced sensing with hyperbolic metamaterial, Adv. Opt. Mater. **7**, 1900680 (2019).

[12] K. V. Sreekanth, M. ElKabbash, R. Medwal, J. Zhang, T. Letsou, G. Strangi, M. Hinczewski, R. S. Rawat, C. Guo, and R. Singh, Generalized Brewster angle effect in thin-film optical absorbers and its application for graphene hydrogen sensing, ACS Photon. **6**, 1610 (2019).

[13] D. Hoenig and D. Moebius, Direct visualization of monolayers at the air-water interface by Brewster angle microscopy, J. Phys. Chem. **95**, 4590 (1991).

[14] S. Hénon and J. Meunier, Microscope at the Brewster angle: Direct observation of first-order phase transitions in monolayers, Rev. Sci. Instrum. **62**, 936 (1991).

[15] R. Wang, S. He, S. Chen, and H. Luo, Brewster differential microscopy, Appl. Phys. Lett. **121**, 231103 (2022).

[16] W. Daear, M. Mahadeo, and E. J. Prenner, Applications of Brewster angle microscopy from biological materials to biological systems, Biochim. Biophys. Acta Biomembr. **1859**, 1749 (2017).

[17] T. Kawanishi, The shift of Brewster's scattering angle, Opt. Commun. **186**, 251 (2000).

[18] K. J. Lee and K. Kim, Universal shift of the Brewster angle and disorder-enhanced delocalization of p waves in stratified random media, Opt. Express **19**, 20817 (2011).

[19] C. Bahrim and W.-T. Hsu, Precise measurements of the refractive indices for dielectrics using an improved Brewster angle method, Am. J. Phys. **77**, 337 (2009).

[20] R. Paniagua-Domínguez, Y. F. Yu, A. E. Miroshnichenko, L. A. Krivitsky, Y. H. Fu, V. Valuckas, L. Gonzaga, Y. T. Toh, A. Y. S. Kay, B. Luk'yanchuk *et al.*, Generalized Brewster effect in dielectric metasurfaces, Nat. Commun. **7**, 10362 (2016).

[21] D. R. Abujetas, J. A. Sanchez-Gil, and J. J. Sáenz, Generalized Brewster effect in high-refractive-index nanorod-based metasurfaces, Opt. Express **26**, 31523 (2018).

[22] X. Lin, Y. Shen, I. Kaminer, H. Chen, and M. Soljačić, Transverse-electric Brewster effect enabled by nonmagnetic two-dimensional materials, Phys. Rev. A **94**, 023836 (2016).

[23] Z. Chen, X. Chen, L. Tao, K. Chen, M. Long, X. Liu, K. Yan, R. I. Stantchev, E. Pickwell-MacPherson, and J.-B. Xu, Graphene controlled Brewster angle device for ultra broadband terahertz modulation, Nat. Commun. **9**, 4909 (2018).

[24] M. Oliva-Leyva and G. G. De la Cruz, Unveiling optical in-plane anisotropy of 2D materials from oblique incidence of light, J. Phys.: Condens. Matter **31**, 335701 (2019).

[25] B. Majérus, M. Cormann, N. Reckinger, M. Paillet, L. Henrard, P. Lambin, and M. Lobet, Modified Brewster angle on conducting 2D materials, 2D Mater. **5**, 025007 (2018).

[26] D. Pérez-Francés, G. Santos, J. Resl, M. Losurdo, Y. Gutiérrez, and F. Moreno, $Sb_2S_3$-based optical switch exploiting the Brewster angle phenomenon, Opt. Mater. Express **13**, 3677 (2023).

[27] A. H. Castro Neto, F. Guinea, N. M. R. Peres, K. S. Novoselov, and A. K. Geim, The electronic properties of graphene, Rev. Mod. Phys. **81**, 109 (2009).

[28] P. A. D. Gonçalves and N. M. Peres, *An Introduction to Graphene Plasmonics* (World Scientific, Singapore, 2016).

[29] O. V. Kotov and Y. E. Lozovik, Enhanced optical activity in hyperbolic metasurfaces, Phys. Rev. B **96**, 235403 (2017).

[30] O. Y. Yermakov, D. V. Permyakov, F. V. Porubaev, P. A. Dmitriev, A. K. Samusev, I. V. Iorsh, R. Malureanu, A. V. Lavrinenko, and A. A. Bogdanov, Effective surface conductivity of optical hyperbolic metasurfaces: From far-field characterization to surface wave analysis, Sci. Rep. **8**, 14135 (2018).

[31] A. Hrinchenko and O. Yermakov, Designing optical hyperbolic metasurfaces based on gold nanodisks, J. Phys. D: Appl. Phys. **56**, 465105 (2023).

[32] D. I. Yakubovsky, A. V. Arsenin, Y. V. Stebunov, D. Y. Fedyanin, and V. S. Volkov, Optical constants and structural properties of thin gold films, Opt. Express **25**, 25574 (2017).

[33] K. Novoselov, A. Mishchenko, A. Carvalho, and A. Castro Neto, 2D materials and van der Waals heterostructures, Science **353**, aac9439 (2016).

[34] C. Liu, H. Chen, S. Wang, Q. Liu, Y.-G. Jiang, D. W. Zhang, M. Liu, and P. Zhou, Two-dimensional materials for next-generation computing technologies, Nat. Nanotechnol. **15**, 545 (2020).

[35] I. Malkiel, M. Mrejen, A. Nagler, U. Arieli, L. Wolf, and H. Suchowski, Plasmonic nanostructure design and characterization via deep learning, Light Sci. Appl. **7**, 60 (2018).

[36] C. Majorel, C. Girard, A. Arbouet, O. L. Muskens, and P. R. Wiecha, Deep learning enabled strategies for modeling of complex aperiodic plasmonic metasurfaces of arbitrary size, ACS Photon. **9**, 575 (2022).